Journal of Structural Geology 30 (2008) 777–790

Contents lists available at ScienceDirect

Journal of Structural Geology

journal homepage: www.elsevier.com/locate/jsg

Dynamic recrystallization of garnet and related diffusion processes

Michel Bestmann [a], Gerlinde Habler [b,*], Florian Heidelbach [c], Martin Thöni [b]

[a] GeoZentrum Nordbayern, University Erlangen/Nuremberg, 91054 Erlangen, Germany
[b] University of Vienna, Althanstrasse 14, 1090 Vienna, Austria
[c] Bayerisches Geoinstitut, University Bayreuth, 95440 Bayreuth, Germany

ARTICLE INFO

Article history:
Received 25 May 2007
Received in revised form 6 February 2008
Accepted 7 February 2008
Available online 4 March 2008

Keywords:
Garnet
Plastic deformation
Recrystallization
Diffusion
Electron backscatter diffraction

ABSTRACT

Electron backscatter diffraction and compositional data of Permian metapegmatite garnet from the Koralpe basement (Eastern Alps, Austria) show the evolution of distinct intracrystalline shear zones in c. 10 mm sized almandine–spessartine garnet. Orientation maps reveal continuous distortion of the crystal lattice. New garnet grains (grain size 20–30 μm) within intragranular deformation zones, oriented subparallel to the main foliation of the metapegmatite, have similar crystal orientations to the host garnet, whereas recrystallized grains along fractures or along growth heterogeneities show a much weaker crystallographic preferred orientation (CPO). Needles of kyanite as well as inclusions of apatite, xenotime and rutile occur along the deformation zones. Together with the Ca variation across the deformation zones these inclusions give evidence of material diffusion related to crystal plastic deformation of garnet. The individual garnet porphyroclasts record the evolution of recrystallization microfabrics. New grains, once formed by subgrain rotation recrystallization, are able to deform partly by diffusion accommodated grain boundary sliding resulting in a weakening of the CPO. Whereas magmatic garnet growth had taken place at LP conditions in equilibrium with andalusite, the occurrence of kyanite in some deformation zones, triggered by the localized crystal plasticity of garnet, indicates that the deformation was related to the Cretaceous HP metamorphic event.

1. Introduction

Garnet is stable over a wide range of PT conditions and bulk compositions and thus is ubiquitous in several rock types of the Earth's crust and mantle. It is therefore of particular interest to obtain knowledge of its deformation mechanisms. In the last 15 years the deformation behavior of garnet was controversially discussed. Den Brok and Kruhl (1996) and Ji and Martignole (1994) showed that there is considerable debate in the interpretation of garnet microstructures with respect to plastic deformation versus diffusion processes controlling deformation of garnet under natural conditions. Thus far, well-constrained examples of plastically deformed garnets are rare. The presence of garnet sub-structure must not be *a priori* related to intracrystalline plastic deformation mechanisms. Trepmann and Stöckhert (2002) interpreted deformation microfabrics (microstructures and related crystallographic orientation data) within elongated and sub-structured eclogite garnets from the Sesia Zone of the Alps being due to cataclastic fragmentation during seismic loading and postseismic creep. Another kind of garnet sub-structure developed by a mechanism other than deformation may result from amalgamation of independently nucleated garnet grains (Spiess et al., 2001; Wheeler et al., 2001; Prior et al., 2002; Dobbs et al., 2003). However, plastic deformation of garnet has been interpreted on the basis of TEM work for naturally deformed garnets (e.g. Voegele et al., 1998a; Ji and Martignole, 1994) and for experimentally deformed garnets (e.g. Voegele et al., 1998b; Li et al., 2006). Indirect evidence of plastic deformation was given by Kleinschrodt and co-workers (Kleinschrodt and McGrew, 2000; Kleinschrodt and Duyster, 2002) for elongated garnets within granulite-facies quartzites from Sri Lanka which show a weak crystallographic preferred orientation (CPO) but exhibit little sub-structure. Prior et al. (2000) related sub-structures of mantle garnets to high-temperature dislocation creep and recovery. For a long time the key question remained whether garnet may undergo dynamic recrystallization during deformation similar to other rock forming minerals (Urai et al., 1986; Urai and Jessell, 2001). Recently Storey and Prior (2005) presented the first direct evidence of dynamic garnet recrystallization and associated subgrain formation by means of electron backscatter diffraction (EBSD) analyses from elongated garnets from NW Scotland deformed under amphibolite facies conditions at c. 700 °C. The authors suggest a strain dependent evolution of individual garnet porphyroclasts starting from dislocation creep and recovery, followed by dynamic recrystallization by subgrain rotation and finally

* Corresponding author. Tel.: +43 1 4277 53475; fax: +43 1 4277 9534.
E-mail address: gerlinde.habler@univie.ac.at (G. Habler).

0191-8141/$ – see front matter © 2008 Elsevier Ltd. All rights reserved.
doi:10.1016/j.jsg.2008.02.007

diffusion creep assisted grain boundary sliding of former recrystallized grains.

In this study we present microstructures and related compositional data in order to understand garnet recrystallization due to plastic deformation and associated diffusion processes. EBSD and electron microprobe (EMP) data of a garnet-bearing Permian metapegmatite (sample 04T26K) from the Austroalpine Koralpe basement in the Eastern Alps (Austria) show the evolution of intracrystalline shear zones in coarse-grained metapegmatite garnet with a well-developed grain and subgrain microstructure. Deformational microstructures are correlated with major element compositional changes during garnet recyrstallization, as well as with associated crystallization processes of accessory inclusions.

2. Geological setting

The Saualpe–Koralpe Complex is part of the Austroalpine basement units east of the Tauern Window in the Eastern Alps (Fig. 1). Lithologically it consists mainly of poly-metamorphic siliciclastic meta-sedimentary rocks with subordinate marbles and intercalations of meta-gabbros, eclogites, eclogite–amphibolites and metapegmatites. The dominating tectonometamorphic imprint was established during Upper Cretaceous eclogite–facies metamorphism (Miller and Thöni, 1997) and subsequent exhumation. Relic pre-Cretaceous mineral assemblages in metapelites indicate an early low-pressure metamorphic imprint, which was related to the Permian magmatic event (Schuster et al., 2001; Habler and Thöni, 2001). Pegmatite intrusion had occurred between 285 and 225 Ma forming widespread meter- to tens-of-meters-sized bodies in Al-rich metapelites (Thöni and Miller, 2000; Habler et al., 2007). The major deformation of the pegmatites and their surrounding rocks occurred during Cretaceous eclogite facies metamorphism and subsequent exhumation. PT constraints are not available from the immediate sampling location, but for different parts of the Koralpe basement peak PT conditions were given at 600–650 °C/1.8–2.0 GPa (Miller and Thöni, 1997), 640–720 °C at presumed 2.4 GPa (Miller et al., 2007) and 700–750 °C/1.5–1.6 GPa (Gregurek et al., 1997) for eclogites using various thermodynamic data. PT estimates from metapelitic rocks range at 700 ± 50 /1.4–1.6 GPa (Gregurek et al., 1997) and 700 ± 68/1.5 ± 0.15 to 600 ± 63 °C/1.0 ± 0.15 GPa (Tenczer and Stüwe, 2003). The P-variations may be interpreted as due to either the existence of tectonic subunits that passed different PT paths during the Cretaceous HP event, or equilibration at different stages of the exhumation path.

All data presented here were obtained from sample *04T26K*, which stems from the locality Wirtbartl in the southern Koralpe (geographic coordinates: 5177709 N, 504737 E; UTM zone 33N, geodetic datum: WGS84), where metapegmatites form intercalations in Al-rich metapelites with characteristic kyanite paramorphs after andalusite (Habler et al., 2007; Thöni et al., in press).

3. Analytical methods

3.1. Sample preparation

Optical microscopy, EBSD and EMP measurements were carried out on polished thin sections cut perpendicular to the deformation foliation. The thin sections were SYTON-polished (Fynn and Powell, 1979; Lloyd, 1987; Prior et al., 1996) and carbon coated for EBSD and EMP analysis.

3.2. EBSD analysis

Full crystallographic orientation data were obtained from automatically indexed EBSD patterns collected in a LEO (Zeiss) Gemini 1530 scanning electron microscope fitted with a thermionic field emission gun (Schottky emitter). Working conditions for automated beam scans were: 30 kV acceleration voltage, 4 nA beam current and 20 mm working distance. The EBSD patterns were indexed by using the program CHANNEL 5.03 from HKL software. The center of 7–8 Kikuchi bands was automatically detected using the Hough transform routine (Schmidt et al., 1991; Adams et al., 1993) with a resolution of 120 (internal Hough resolution parameter in the software). The solid angles calculated from the patterns were compared with a match unit of almandine containing 80 reflectors to index the patterns.

The accuracy of individual EBSD orientation measurements is better than 1°. 2° is the minimum misorientation angle between adjacent points that can be reliably identified (Prior, 1999; Humphreys et al., 2001). The misorientation angle was calculated by selecting the minimum misorientation angle and its corresponding axis from all possible symmetric variants (Wheeler et al., 2001).

EBSD orientation data are presented as processed orientation maps. Non-indexed points were partly replaced by the most common neighboring orientation. The degree of processing required to fill non-indexed data points in this way, without introducing artifacts, was tested carefully by comparing the resulting orientation map with the pattern quality map, which represents the grain boundary network (Bestmann and Prior, 2003).

3.3. Grain size analysis

Grain size (gs) distributions were analyzed by means of the EBSD orientation maps (step size 2 μm). Grains were automatically identified by the EBSD software CHANNEL 5 and measured when completely surrounded by boundaries with misorientation angles

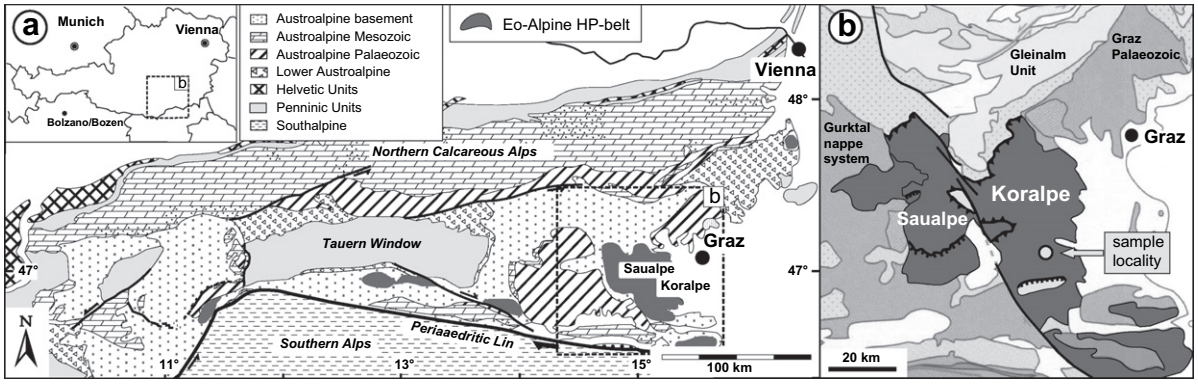

Fig. 1. Tectonic map of (a) the Eastern Alps (modified after Frey et al., 1999) and (b) the Saualpe–Koralpe Complex (modified after Schmid et al., 2004, and Faryad and Hoinkes, 2003).

>10°. Two-dimensional grain size is calculated as the diameter of a circle of equivalent area to the measured grain and is presented as frequency distribution.

3.4. Electron microprobe analyses

Compositional data were measured on a Cameca SX100 electron microprobe at the Department of Lithosphere Research (University of Vienna, Austria). Natural and synthetic silicates and oxides were used as standard material and a PAP routine was applied for matrix correction (Pouchou and Pichoir, 1991). Measurement conditions during single point analyses were at 15 kV accelerating voltage and 20 nA beam current. Garnet analyses were performed with a focused beam whereas for plagioclase and mica analyses a defocused electron beam of 5 μm diameter was used. Element distribution maps were generated at 20 kV accelerating voltage and a dwell time of 100 ms for each data point, using a focused electron beam. Scanning was performed with 1 μm steps using stage-controlled static mode (no stage movement during the measurement).

4. Microfabric data

4.1. Metapegmatite microstructures

The Permian magmatic growth of cm-sized almandine–spessartine garnet (Fig. 2a; Section 5.1.) occurred in equilibrium with coarse-grained andalusite, plagioclase (oligoclase), K-feldspar, quartz, muscovite, tourmaline and very fine to ultra-fine-grained accessory phases (Mg–Na-bearing Ca-phosphate + xenotime + ilmenorutile–struverite ± zircon ± monazite ± corundum ± sphalerite ± uraninite). In general the coarse-grained magmatic major phases largely have preserved their euhedral grain shapes, whereas the magmatic accessory phases occur as very fine-grained (gs 10–50) or ultra-fine-grained (gs <1 μm) inclusions in the coarse-grained phases. During the Cretaceous HP metamorphic overprint, deformation zones were formed in the pegmatitic quartz–feldspar domains and the resultant flow fabric is deflected around the c. 10 mm sized garnet grains. Strain is mainly accommodated in the pegmatitic matrix consisting of dynamically recrystallized quartz (gs 40–200 μm), feldspar (gs 40–100 μm), kyanite, tourmaline, apatite and localized thin layers of fine-grained muscovite, which all form a compositional layering. Dynamic recrystallization by predominant grain boundary migration and subordinate subgrain rotation caused grain size reduction of magmatic quartz and both feldspars, and produced an inequigranular interlobate fabric. Grain boundaries of both medium- and fine-grained quartz and feldspar are smoothly curved. Magmatic feldspar relics have rounded grain shapes and show lattice distortion, deformation bands and deformation twins as well as subgrain formation. They frequently display core and mantle microstructures. In fine-grained recrystallized domains feldspar developed a SPO. The lack of a polygonal quartz–feldspar fabric therefore speaks against significant static recrystallization.

The metamorphic assemblage of the metapegmatites consists of quartz + plagioclase (albite) + K-feldspar + muscovite + kyanite ± garnet ± tourmaline + accessory phases (apatite + xenotime + rutile). Metamorphic garnet is confined to very rare 10–50 μm sized overgrowths on magmatic garnet in contact with plagioclase, and does not form new nuclei in the matrix.

4.2. Garnet microfabrics

4.2.1. Crystallization microstructures

Garnet porphyroclasts are equant and display oscillatory and sector zoning of idiomorphic growth domains reflected by variations in the color intensity and the distribution of ultra-fine-grained accessory inclusions (Fig. 2a). Most garnet grains show a weakly colored rim which is separated from the strongly colored core by a quartz-inclusion rich zone (Fig. 2b). Garnet crystallization is not strictly concentric. Intergrowths of garnet with euhedral kyanite paramorphs after andalusite and oligoclase indicate equilibrium crystallization due to the grain size compatibility (Clarke et al., 2005; Habler et al., 2007).

4.2.2. Deformation microfabrics

Only few garnets of the metapegmatite show internal deformation microstructures, which are developed to strongly variable degree even within single thin sections (Fig. 2a). Whereas some grains do not show any significant grain internal deformation, adjacent grains may display numerous intragranular shear zones. Garnet deformation microstructures observable under the light optical microscope are confined to two samples, whereas the majority of the metapegmatite garnets solely display variably oriented microfractures or trails of recrystallized inclusions (Habler et al., 2007). EBSD investigations reveal that some, but not all of these microstructures show evidence of lattice distortion and subgrain microstructures. Intergranular deformation zones occur in domains where two adjacent garnet grains adjoin (Habler et al., 2007), whereas intragranular deformation zones crosscut both the core and rim of magmatic garnet.

In the following we present representative deformation microstructures of one garnet grain (garnet-2, grt-2) from sample *04T26K* (Fig. 2). Grt-2 contains several different orientation domains which are separated by fractures. The misorientation between the domains is up to 53°. Several distinct deformation zones within the different orientation domains of grt-2 were analyzed.

The presented garnet microstructure contains a heterogeneous deformation fabric and is characterized by distinct intragranular deformation zones (Figs. 2a, 3 and 4).

Two main orientation domains are separated by a fracture with an average misorientation of 25° between domains A and B. Domain-A (violet-blue) shows only slight lattice distortion up to 5° and is nearly free of subgrain boundaries >2° (Fig. 4a,c). Domain-B (blue) is heterogeneously deformed. Orientations along linear transects (misorientation profiles, Fig. 4b) reveal progressive rotational lattice distortion patterns (up to 35° misorientation dispersion) towards the deformation zones (Fig. 5a,b). Even if dispersion paths of individual misorientation profiles may show a clear rotation axis around a specific crystallographic direction, the rotation axis varies for different misorientation profiles within the distorted domain-B and also for other grt-2 domains. Subgrain boundaries crossed by individual misorientation profiles have some influence on the dispersion geometry but do not significantly change the dispersion path (Fig. 5c,d). The statistical distribution of misorientation axes of subgrain boundaries within domain-B is random (Fig. 6a). The crystallographic dispersion across grain boundaries between small grains and host is lost as soon as these grains are completely surrounded by boundaries >10° (high-angle boundary), referred to as individual new grains (Storey and Prior, 2005). This trend of continuous rotational lattice distortion and sudden loss of crystallographic control across grain boundaries into new grains is evident in Fig. 5c,d.

Four different intragranular deformation zones have been distinguished by means of the microstructural appearance and their position within the garnet (Fig. 4).

(I) Deformation zones I (Figs. 2b, 3a,b and 4) are characterized by small new grains (gs 5–25 μm, Fig. 7) aligned as single chains (bands) parallel to each other. These deformation zones I do not correlate with fractures and are oriented parallel to the deformation foliation of the matrix. A relatively high density of subgrain boundaries accompanies these deformation zones. Subgrains have the same size (gs 5–25 μm) as new grains.

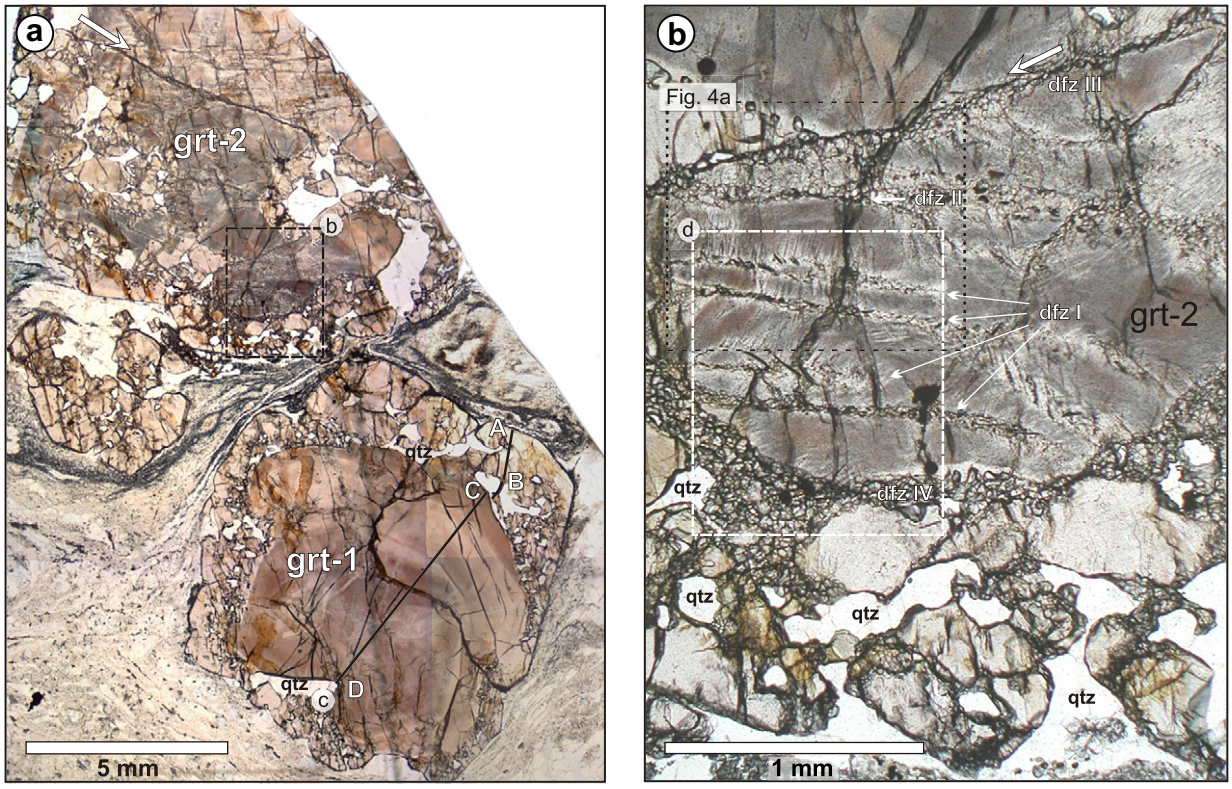
a
grt-2
grt-1
qtz
A
B
C
D
5 mm
b
Fig. 4a
dfz III
dfz II
dfz I
dfz IV
grt-2
qtz
1 mm

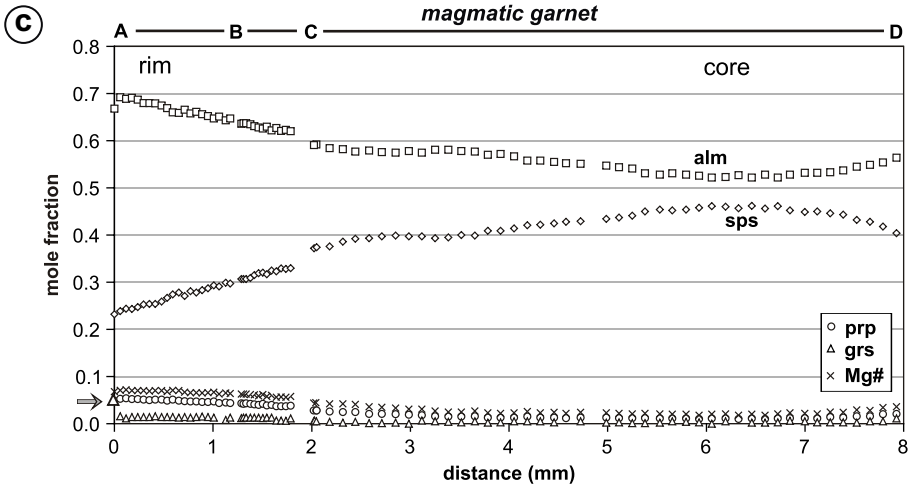
c
magmatic garnet
A B C D
rim
core
alm
sps
prp
grs
Mg#
mole fraction
distance (mm)

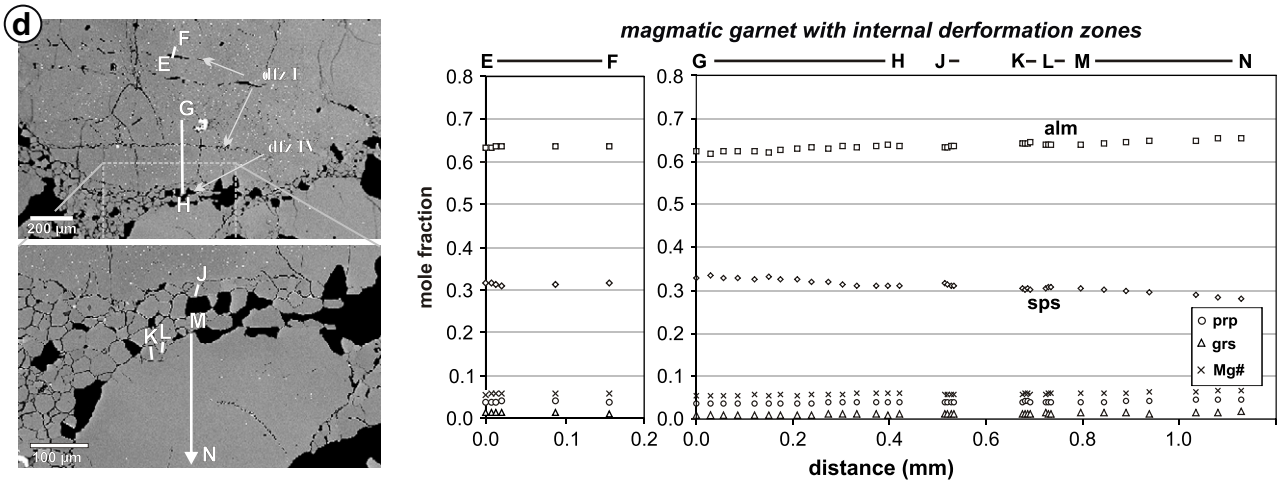
d
E F G H J K L M N
dfz I
dfz IV
200 µm
100 µm
magmatic garnet with internal derformation zones
alm
sps
prp
grs
Mg#
mole fraction
distance (mm)

The CPO of the new grains is similar to the surrounding distorted host (Fig. 4d).

(II) Deformation zone II contains aggregates of new small grains. Relics of the deformed host domain display a subgrain mosaic with a similar size distribution as the surrounding new grains (gs 10–40 μm, Fig. 7). The deformation zone II is oriented subparallel to the deformation zone I. The orientation distribution of the new grains shows a higher scattering around the host orientation than in the deformation zones I (Fig. 4d). The maxima are weaker and located further away from the host.

(III) Deformation zone III is characterized by a coarser grain size (gs >25 μm) of new grains compared to deformation zones I and II (Fig. 7). Relics of deformed host domains are rare. A part of deformation zone III follows a fracture (IIIa), which separates domain-A from domain-B. Domain-A does not show any pronounced lattice distortion pattern adjacent to the deformation zone. By contrast, domain-B adjacent to the deformation zone III reveals strong lattice distortion (Fig. 4c) and is characterized by a subgrain mosaic (Figs. 3a and 4a,b). The subgrains have a smaller average, grain size range (gs 5–30 μm) as the new grains (gs 5–50 μm, Fig. 7). The CPO of new grains is very weak, but the maxima, especially of <100>, still fall together with the host orientation (Fig. 4d).

(IV) The transition zone between the garnet core and the quartz-inclusion rich garnet rim is characterized by deformation zone IV with variable amount of new grains (gs 5–50 μm, Fig. 7) and distorted relics of the host domain. Few quartz grains (gs 20–70 μm) occur in between the new garnet grains (Fig. 2d). The garnet core and the quartz-inclusion rich garnet rim have a similar crystallographic orientation with an average misorientation of 15° across the deformation zone IV. The microstructure of deformation zone IVa with its relics of distorted host domain is comparable with the microstructure of the deformation zone II. Subgrain formation is evident in these domains and also in the adjacent deformed host. The CPO of new grains shows a wide scatter around the host orientation (Fig. 4d). Deformation zone IVb contains a higher amount of new grains. The CPO is very weak (Fig. 4d), but the <100> maxima still reflect the host orientation.

In general, new grains of all types of deformation zones show a homogeneous internal crystallographic orientation (lattice distortion <1°). Few of these grains contain subgrain boundaries. The distribution of misorientation angles measured between new grains and the neighboring host grain reveal a higher content of boundaries with 10–25° misorientation for the deformation zones I, compared to the deformation zones II–IV where grain boundaries >25° predominate (Fig. 6b). Boundaries >25° dominate deformation zone II. At the same time boundaries <25° are more frequent than in deformation zones III and IV. The same trend of misorientation angle distribution is given between neighbor-pairs of new grains themselves (Fig. 6c). The distribution of neighbor-pair misorientation axes between host and new grains, as well as between new grains themselves, is for all deformation zones close to random (Fig. 6b,c).

4.2.3. Inclusions

The strongly colored garnet core domains outside the deformation zones contain numerous <1 μm-sized inclusions of xenotime, Mg–Na-bearing Ca-phosphate and ilmenorutile–struverite (Nb–Ta–Sn-bearing Ti-phases), whereas the colorless garnet rim has a significantly lower density of ultra-fine-grained inclusions. Within the deformation zones phosphate inclusions have larger grain sizes (gs 10–30 μm) than in undeformed garnet domains (Fig. 3e,f). Garnet host domains displaying a strong lattice distortion immediately adjacent to the deformation zones are nearly inclusion-free, which is reflected by bleached host domains adjacent to the deformation zones. Similarly bleached garnet zones accompany straight to weakly curved trails of very fine-grained inclusions (corundum, rutile, xenotime, white mica) in core domains of microscopically undeformed garnet grains. The fine-grained inclusion trails have variable spatial orientation.

Acicular kyanite grains (determined by EBSD analysis) 20–150 μm in length are associated with deformation zones I, and have a preferred orientation subparallel or slightly oblique relative to these deformation zones (Fig. 3b).

5. Major element compositional data

5.1. Garnet

Coarse-grained euhedral garnet has almandine–spessartine composition (Fig. 2c), which is characteristic for magmatic pegmatite garnet (Whitworth and Feely, 1994). The Mn-content continuously decreases from 46 mol% spessartine in the core to 23 mol% at the rim, whereas Mg slightly increases (up to 6 mol% pyrope component) from the core to the rim at consistently very low Ca-content (up to 1.5 mol% grossular component). The Fe content behaves inversely relative to Mn. Oscillatory color zoning patterns are not reflected by the major element garnet composition, and even crystallization microstructures displayed by quartz-inclusion rich garnet zones are not related to a significant compositional hiatus. Only the outermost 10–50 μm of garnet porphyroclasts may show a significant increase in the Ca content up to 15 mol% grossular component.

Detailed quantitative analyses of the garnet core domains showed that new grains of intragranular deformation zones have a similar major element composition as the unaffected magmatic garnet host (Fig. 2d). A slight increase in Ca content of the new grains and subgrains is generally below the analytical error of standard EMP analysis. Furthermore, element distribution maps (Fig. 3c,e,f) and compositional profiles (Fig. 3d) reveal a slight, but significant depletion of the grossular component by <0.5 mol% in the host garnet adjacent to the deformation zones. Although the absolute variations are very low, the relative trends of Ca enrichment in the small grains and Ca depletion in the adjacent host garnet are evident (Fig. 3d).

The Mn content decreases continuously across the deformation zones from the core to the rim of magmatic garnet (Fig. 2d). No systematic Mn variations related with the intragranular deformation zones have been observed.

6. Discussion

6.1. Crystal plastic deformation of garnet

Storey and Prior (2005) present for the first time direct evidence of plastic deformation and dynamic recrystallization processes of

Fig. 2. (a, b) Photomicrograph of metapegmatite (*04T26K*; plane polarized light). (a) The color zoned garnet core is surrounded by a weakly colored quartz-inclusion rich growth rim. The thick white arrow marks a prominent fracture accompanied by a well-developed (sub)grain microstructure in grt-2. Black lines with capital letters give the position of the compositional profile (c). (b) Detail of (a) grt-2. Different deformation zones dfz I–IV with well-developed (sub)grain microstructure are marked by white arrows (see text and Fig. 4b). (I, II) Deformation zones parallel to main foliation of the metapegmatite, (III) fracture related deformation zone, and (IV) deformation zone at the transition between garnet core and quartz-inclusion rich outer zone. (c) Major element compositional profile of the garnet crystal showing continuous growth zoning. Oscillatory color zoning patterns do not correspond to the garnet composition. The arrow at point A indicates the slight increase in Ca content at the outermost margin. (d) Left: BSE images of dfz IV in garnet of Fig. 2b. Black phases in the deformation zone are quartz. Capital letters and white lines mark the compositional profile at the right hand side. Right: Major element compositional profile of garnet across dfz I and dfz IV. Note the continuous Mn–Fe zoning. This figure can be viewed in color in the online version of this article.

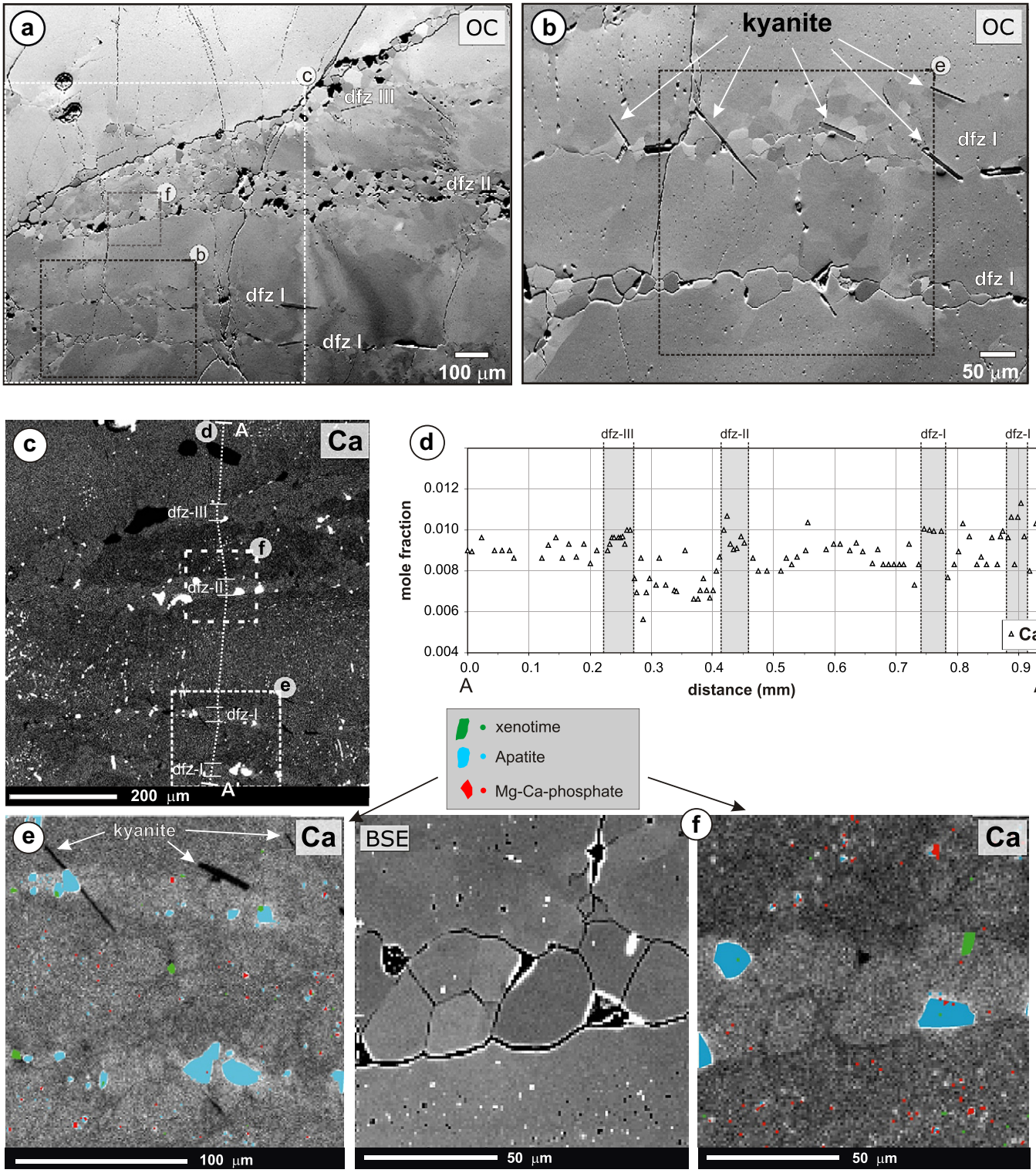

Fig. 3. (a, b) SEM orientation contrast (OC) images of different intragranular deformation zones in garnet grt-2 (dfz I–III; see text and Figs. 2 and 4b). Acicular kyanite inclusions are restricted to dfz I. Note some kyanite needles cross cut the deformation zone. Black spots are related to pores/voids due to thin section preparation. (c) Ca distribution map of the garnet core domain. (d) Strongly inflated Ca profile across deformation zones (dfz I–III). Absolute variations are below the analytical error of the EMP analysis, but relative trends correlate with the Ca distribution map given in (c). (e, f; right) Detailed Ca distribution maps and BSE image (f; left) of the quadrangles marked in (a) and (c). Inclusions are highlighted by symbols. Note that inclusions in deformation zones are coarser (10–30 μm) than in the unaffected garnet core (<1 μm). Inclusion-free host garnet adjacent to shear zones is depleted in Ca. This figure can be viewed in color in the online version of this article.

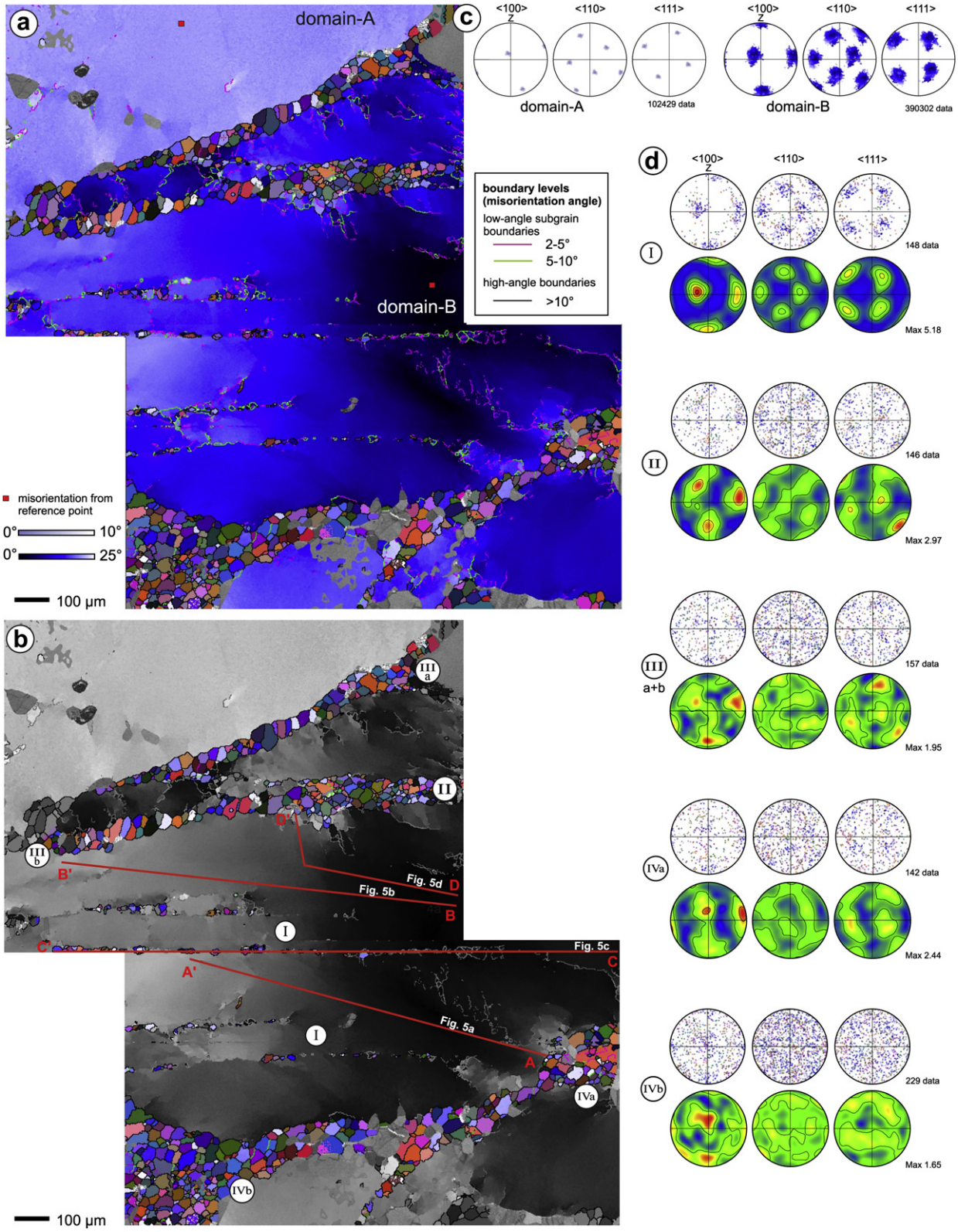

Fig. 4. (a, b) EBSD orientation maps (processed) of the grt-2 microstructure. Grt-domains A and B are color-shaded according to their angular misorientation from the points marked as red squares. Gray pixels are non-indexed points or other phases than garnet. Data are on a grid with 2 µm spacing. Boundary levels are color-coded (see key). (b) Orientation map. Intragranular deformation zones with new grains are highlighted. Red lines represent locations of misorientation profiles, displayed in Fig. 5. (c) Orientation of domain-A and domain-B presented as pole figures (equal area upper hemisphere stereoplots). (d) Orientations of new small grains within intragranular deformation zones I–IV are given as pole figures (1 point per grain plots + contoured plots, half width 20° and cluster size 5°; contour lines are multiples of mean uniform density + maximum value is given): (I) initial deformation zone, (II) progressed deformation zone, (III) fracture related deformation zone, and (IV) deformation zone at the transition between garnet core and quartz-inclusion rich outer zone.

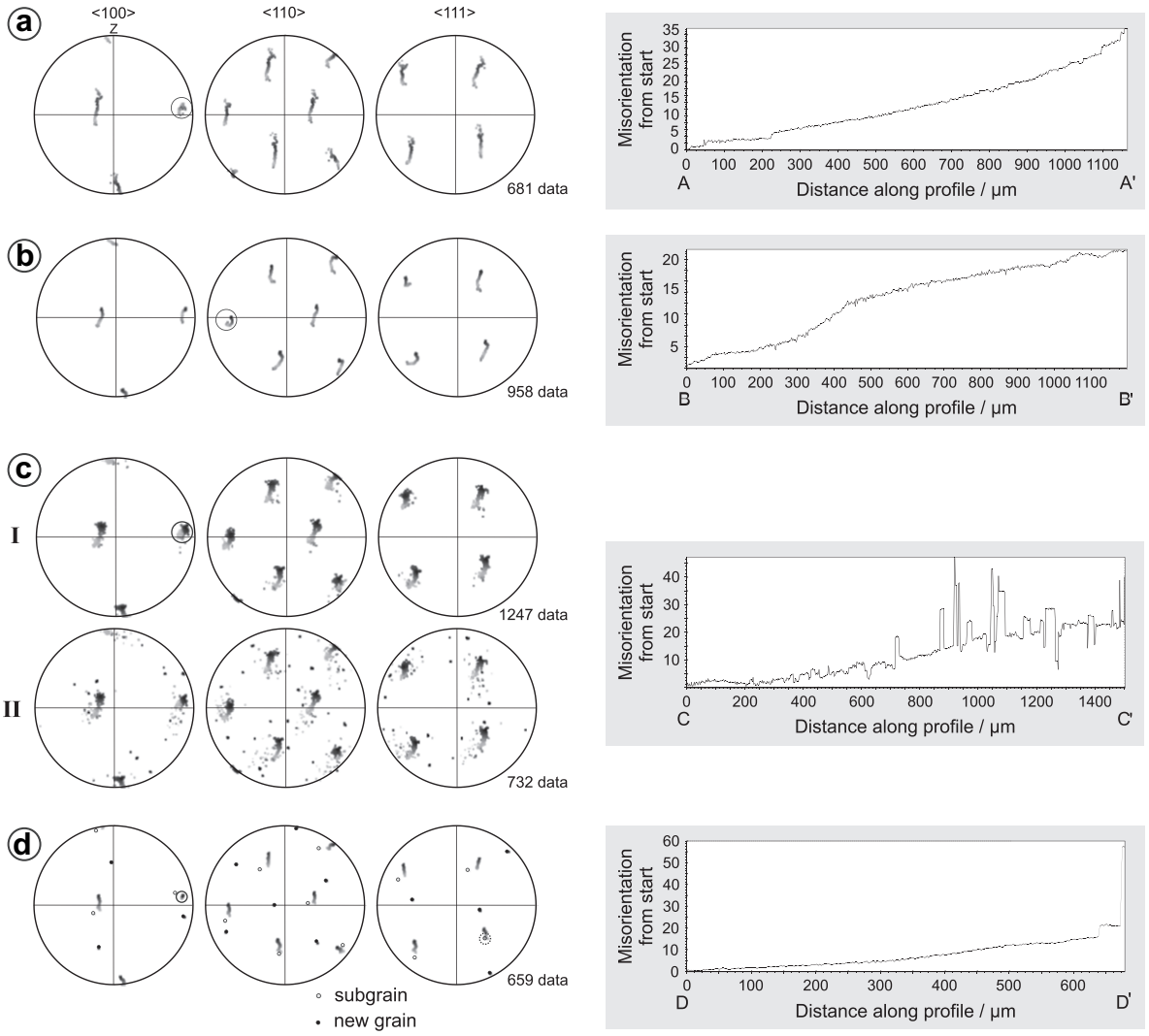

Fig. 5. (a–d) Changes of the orientation along misorientation profiles (marked in Fig. 4b) are shown as dispersion patterns in pole figures and as misorientation angle with respect to starting point. Pole figures of (c) represent orientation along line C without (I) and including new recrystallized grains (II). Possible rotation axes for dispersion data are marked with a circle. For (d) also the possible misorientation axis across the subgrain boundary is marked with a dotted circle.

garnet porphyroclasts affected by various strain intensities. In their case the strain dependent microstructure, ranging from lattice bending towards subgrain formation and dynamic recrystallization, is distributed across a complex arrangement of different garnet morphologies.

In contrast, within the Koralpe metapegmatite a similar microstructural inventory is located towards distinct and well-developed intracrystalline deformation zones within a single garnet porphyroclast. Recently Bestmann and Prior (2003) discussed the development of intragranular deformation zones accompanied by dynamic recrystallization by means of EBSD data for calcite marble. They show that such a microstructural scenario is best suitable to study deformation, recovery and recrystallization mechanisms to understand strain localization and the accompanied processes to develop new dynamically recrystallized grains.

6.1.1. Dislocation creep, recovery and subgrain rotation recrystallization

Lattice deflection with rotational orientation dispersion around rational crystallographic axes towards the deformation zones (Fig. 5a,b) gives clear evidence of crystal plastic deformation by dislocation creep within the garnet host (Lloyd and Freeman, 1994; Lloyd et al., 1997; Prior et al., 2002; Bestmann and Prior, 2003; Storey and Prior, 2005). Since subgrain boundaries do not show a strong influence on the general dispersion path along individual orientation transects (Fig. 5c) it seems reasonable that, with increasing strain, recovery has formed subgrain walls. Subgrain boundaries do not correspond to fractures, thus brittle development of the dispersion path as discussed for garnet porphyroclasts by Trepmann and Stöckhert (2002) can be excluded for the material investigated. Random misorientation axes of subgrain boundaries (Fig. 6a) suggest that plastic deformation was accommodated by several slip systems operating contemporaneously (Leiss and Barber, 1999; Bestmann and Prior, 2003). Further strain has produced a continuous increase in misorientations by subgrain rotation (Bestmann and Prior, 2003; Storey and Prior, 2005). The high number of new grains of deformation zone I with misorientation angles between 10° and 25° (Fig. 6) and the small scattering angle of new grains around the host orientation (Fig. 4) give evidence of host-controlled dynamic recrystallization. The similar size of subgrains with new small grains within and adjacent to deformation zones is consistent with subgrain rotation recrystallization. In other words subgrain rotation recrystallization created new small garnet grains from pre-existing subgrains.

However, recovery and subgrain rotation cannot explain the random orientation of the misorientation axes between small

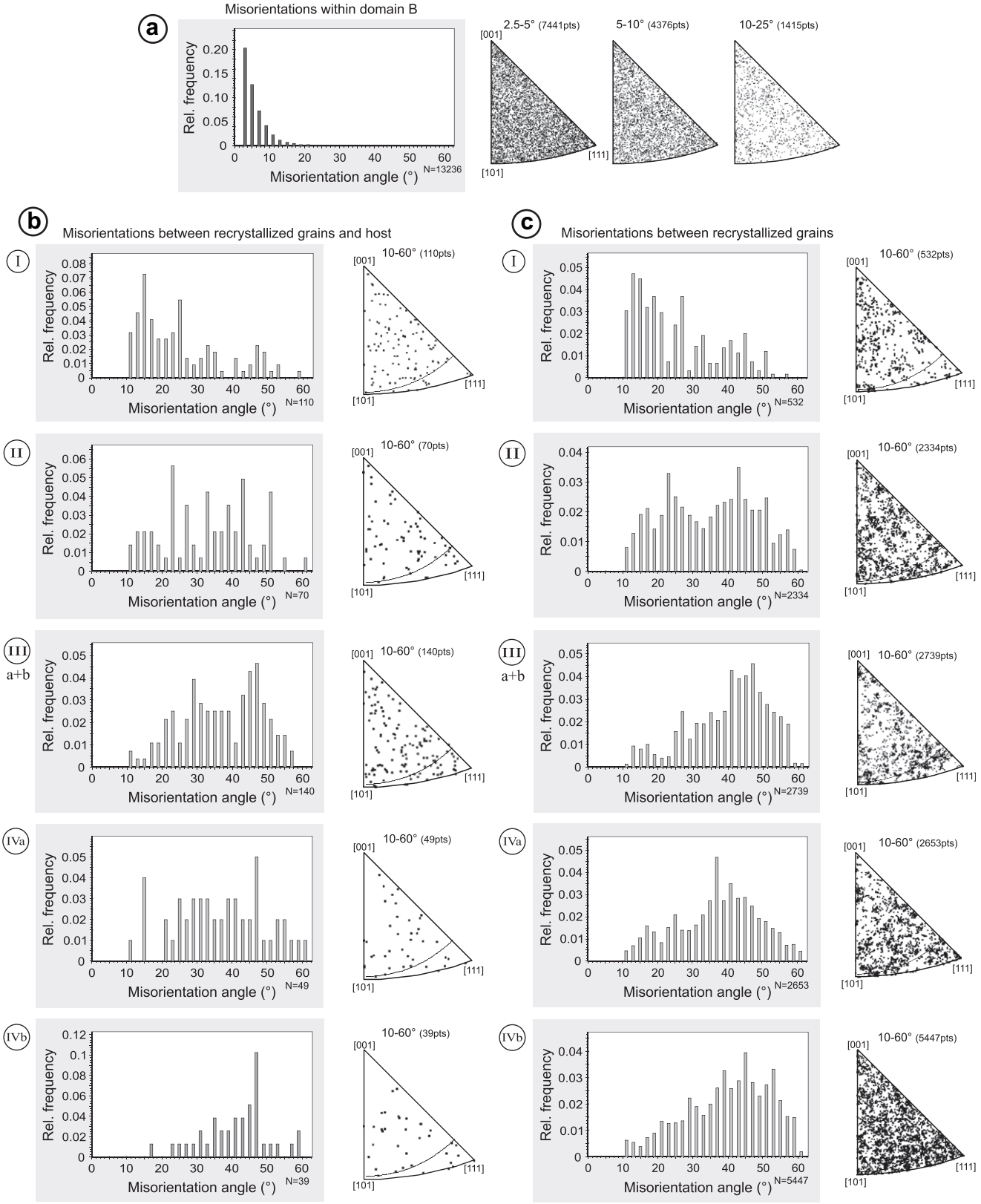

Fig. 6. Distribution of misorientation angles (histogram, left) and axes with respect to the crystallographic reference system (inverse pole figures, right). (a) Misorientations for intragranular subgrain boundaries of domain B (automatically detected). (b) Misorientations of grain boundaries (>10°) between recrystallized grains and host (manually detected, one per grain). (c) Misorientations of grain boundaries between recrystallized grains within deformation zones I–IV (automatically detected).

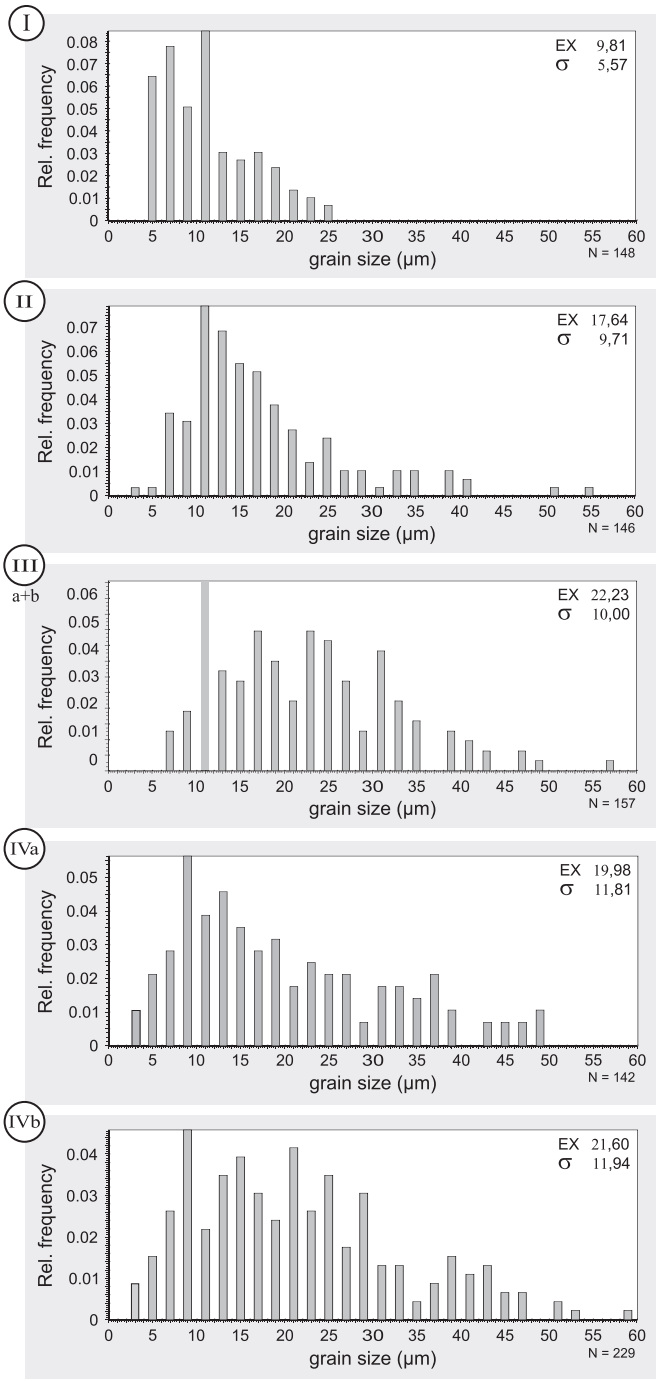

Fig. 7. Grain size distribution of new grains within deformation zones I–IV. Number of grains (N), average grain size (EX) and standard deviations (σ) is given.

new grains and their host, and the considerably larger than 25° misorientation angles in deformation zones II, III and IV.

6.1.2. Grain boundary sliding

Large rotation angles and randomly oriented misorientation axes between porphyroclasts and recrystallized grains has been referred to as non host-controlled recrystallization (Jiang et al., 2000; Kruse et al., 2001). The new data can be explained by the following scenario. New grains were initially developed by subgrain rotation recrystallization. As soon as high-angle grain boundaries were formed and separate the new grains from the host, these dynamically recrystallized grains were able to undergo grain boundary sliding accompanied by grain rotation, referred as "rotation jump" (Ree, 2000; Bestmann and Prior, 2003). In other words the new grains lose crystallographic control with respect to their host. The sliding process and accompanied grain rotation increases the average misorientation between new grains and host and between neighboring grains themselves and result in randomized misorientation axes and a weakening of the CPO (see also section 6.1.3) (Jiang et al., 2000).

Grain boundary sliding needs an accommodation mechanism like frictional sliding and associated dilatation (Sammis, 2001), diffusion creep (Ashby and Verrall, 1973; Gifkins, 1973, 1976) and/or dislocation creep (Gifkins, 1991, 1994). Randomization of garnet orientation by cataclasis (frictional) deformation processes as suggested by Trepmann and Stöckhert, 2002 can be excluded. Few subgrain boundaries give evidence that new recrystallized grains continued to deform internally by dislocation creep. However, the occurrence of only few subgrain boundaries within the general strain free grains may be related to relatively fast recovery processes accompanied by grain boundary migration (Bestmann et al., 2006). Curved grain boundaries (see dfz IV in Fig. 4b) give evidence of grain boundary migration during deformation (Jessell, 1987). Dislocation creep associated with grain boundary migration is commonly inferred for initial dynamic recrystallization and ongoing mylonitization (Drury et al., 1985; Bestmann and Prior, 2003; Bestmann et al., 2006). Increase of grain size of new grains in the different deformation zones is interpreted to result from stress induced diffusion-controlled growth (see also section 6.1.3) (Bestmann and Prior, 2003; Terry and Heidelbach, 2004; Storey and Prior, 2005). It seems reasonable then that grain size reduction by dynamic recrystallization and associated strain localization leads to a decrease in the importance of grain-size-insensitive (GSI) dislocation creep relative to grain-size-sensitive (GSS) diffusion-accommodated grain boundary sliding (Bestmann and Prior, 2003; Storey and Prior, 2005). Thus we infer that recrystallized grains, once formed, are able to deform and rotate due to a combination of intra-crystalline dislocation creep and diffusion accommodated grain boundary sliding (see also Casey et al., 1998).

6.1.3. Microstructural position of deformation zones and the development of their specific microfabric

In the following we will discuss the evolution of the microfabric, i.e. grain size and different strength of the CPO of the different deformation zones with respect to their microstructural position within the garnet porphyroclast.

The deformation zones I and II are oriented parallel to the deformation foliation of the matrix. Since these deformation zones are not related to any fractures it is likely that the orientation of the deformation zones I and II are related to the crystallographic orientation of domain B and the local flow stress field around the garnet porphyroclasts.

In general, for garnet 1/2 <111> {110} and <100> {010} are the most probable glide systems based on TEM analyses of experimentally and naturally deformed garnets (Karato et al., 1995; Voegele et al., 1998a,b). Even if we do not know the exact flow stress field, around the garnet porphyroclast, which might have caused the internal deformation zones, one of the maxima is in the *Z* direction of the <100> pole figure and thus one of the {010} plane is parallel to the overall foliation of the metapegmatite. In contrast none of the <110> maxima lie in *Z* direction. Accordingly one of the <100> maxima is (sub)parallel to the *X* direction, even if this might not represent the exact shear direction with respect to the deformation zones. However, none of the <111> direction lies in the *XY* plane of the pole figure. Thus even if the pole figure will be rotated around *Z* none of the <111> maxima would ever fall together with the *X*-direction of the pole figure. Therefore it is likely that domain-B was in an easy glide orientation for the <100> {010} slip system. However, EBSD analyses of deformation zones of type I within

another domain of garnet-2, which shows a different orientation compared to domain B, give evidence that this domain might have been in an easy slip orientation for 1/2 <111> {110}slip. It should be pointed out that the misorientation plots for all analyzed domains (see Fig. 6 for domain B) give evidence of the activation of multiple glide systems. Since deformation zone II shows a higher amount of recrystallized grains but also relics of deformed host domains containing a subgrain mosaic similar to deformation zone I, it is suggested that deformation zone II represents the progressed stage of strain localization. With increasing strain the progressive weakening of the initial strong CPO as evident for deformation zone I could be explained by grain boundary sliding accompanied by grain rotation.

Deformation zone III is found to have developed along fractures. The serrate characteristics of the fractures that follow grain boundaries of new recrystallized grains indicate a late opening of these fractures even if they were either pre-existed or synchronously formed with respect to the crystal-plastic deformation (see also Storey and Prior, 2005). Similar fracture related deformation zones are observed within garnet 2 with variable spatial orientation. The deformation zone III is characterized by a coarser grain size and a weaker CPO compared to deformation zones I and II but also contains only a single row of recrystallized grains as is evident for deformation zone I. The processes causing the variations in CPO strength are currently not clear. An initially strong CPO, as observed for the deformation zone I, may have subsequently been weakened due to the progressive evolution of the deformation zone III as suggested for deformation zone II. Nucleation and growth processes along a damage zone, for example, would not necessarily involve the formation of a CPO: The garnet crystal might have undergone localized crystal-plastic deformation accompanied by brittle deformation during a high stress event. Subsequent static recrystallization by nucleation and growth processes may have led to recrystallized grains without marked CPO along these damage zones (Trepmann et al., 2007). In less pronounced damage zones within the garnet the driving force for static recrystallization might have been not high enough for nucleation and growth to occur, leading to restricted static recovery and subgrain rotation recrystallization. However, crystallographic pole figures of all analyzed deformations zones along the variably oriented fractures still show more or less strongly developed maxima related to the host orientation (Fig. 4d). This is in contradiction to a random CPO observed in the deformation experiments of Trepmann et al. (2007) formed as a consequence of stress induced recrystallization within highly damaged zones during subsequent static annealing. Instead it is suggested that the plastic deformation along these fractures was accommodated by the interplay of different glide systems where none of the glide systems was in an easy slip position. This might have led to a higher internal strain energy compared to deformation zones I and might have caused a larger initial "rotation jump" as soon as the new grains evolved to individual grains by subgrain rotation. This would explain the weaker CPO compared to that of deformation zone I. Furthermore, for deformation zones of type III, which are in a less favorable easy slip orientation, a higher dislocation density is likely. Thus, faster syn- and/or post-kinematic grain growth could have caused the coarser grain size of the recrystallized grains compared to those in deformation zones I.

Extensive recrystallization along the transition zone between garnet core and quartz-inclusion rich zone (deformation zone IV) suggests that such growth heterogeneity promoted strain localization. Also for deformation zone type IV it is not clear whether the microfabric, especially the weak CPO, records the progressed stage of strain localization due to ongoing grain boundary sliding, or might be related to extensive stress concentration at heterogeneities and subsequent static recyrstallization by nucleation and growth processes (Trepmann et al., 2007). However, internal subgrain boundaries within recrystallized grains and relicts of deformed host domains favor the first interpretation.

6.2. Garnet composition and its changes during dynamic recrystallization

6.2.1. General garnet composition

In contrast with oscillatory color zoning patterns, the major element composition of garnet shows continuous zoning with Fe behaving inversely relative to Mn (Fig. 2c). Major and trace element compositional as well as Sm–Nd isotopic data indicate that the coarse-grained garnet formation in the Permian pegmatites from the Koralpe resulted from magmatic crystallization (Habler et al., 2007). Temperature conditions during and after garnet growth were apparently too low for major element compositional homogenization to be accomplished. Only some outermost garnet rim domains (10–50 μm), which show a significant increase in the Ca content (arrow at point A of geochemical profile in Fig. 2c), were affected by diffusional re-equilibration during the HP metamorphic overprint (Habler et al., 2007; Thöni et al., in press).

6.2.2. Compositional changes during dynamic recrystallization

Quantitative mineral compositional analyses show that dynamically recrystallized grains of intragranular deformation zones have a nearly identical major element composition as the unaffected magmatic garnet host (Fig. 2d). However, element distribution maps reveal partly a slight but distinct Ca variation (<1 mol%) within and adjacent to the deformation zones (Fig. 3c–f). The Ca variation between the dynamically recrystallized grains and the surrounding host indicates the coherence of compositional variations with the crystal plastic deformation event. Compositional variations are significantly more pronounced within the strongly deformed domain-B than the significantly more weakly deformed domain-A of Grt-2, identified by EBSD analysis (Figs. 3c and 4a). New grains and subgrains show a slight increase in the Ca content with respect to the unaffected garnet host, whereas host domains adjacent to the deformation zones, which represent the optically bleached garnet zones, display a slightly lower Ca content than the primary garnet. The major element distribution in garnet therefore may not be explained by a simple diffusion process.

As one possible explanation, the Ca variations may have resulted from diffusive processes related with apatite crystallization in all types of deformation zones. Whereas relatively larger sized pure apatite (10–30 μm) is present in the deformation zones with new dynamically recrystallized garnet grains, the bleached garnet domain adjacent to the deformation zone is inclusion-free (see also Section 6.2.3.). Na–Mg-bearing Ca-phosphates represent <1 μm sized inclusions in the host garnet unaffected by the deformation. Gradients in chemical potentials during syn-metamorphic deformation may have induced the crystallization of apatite extracting Ca from the garnet host adjacent to the deformation zones. Mg from the primary phosphates may have substituted for Ca in garnet. Still, the slightly elevated grossular content of new dynamically recrystallized garnet grains and subgrains cannot be explained by a single-phase process. A complex evolution of first Ca transport from host garnet into deformation zones and then dynamic recrystallization of new Ca-enriched garnet grains has to be inferred, which seems highly speculative. Overgrowth structures as described by Storey and Prior (2005) from deformation zones in eclogite have not been observed in the present study.

Another possibility for the relative Ca increase in the deformation zones could be the relative immobility of Ca. Other elements may possibly have been expelled by diffusion during the process of dynamic recrystallization, leaving Ca in the deformation zones. However, significant material transport from the matrix into interior garnet domains along the deformation zones can be ruled

out due to the characteristics of Mn zoning. The diffusivity of Mn in garnet is significantly higher than that of Ca (Loomis et al., 1985; Schwandt et al., 1996), and therefore re-equilibration with the matrix should have induced a significant decrease in the Mn content of diffusively affected garnet. However, garnet displays continuous Mn zoning across the deformation zones. Deformation related re-equilibration processes are obviously confined to material exchange between garnet and its inclusions.

6.2.3. Crystallization of inclusions in garnet

The appearance of 20–30 μm sized apatite, xenotime, rutile and kyanite grains is restricted to inclusion trails associated with bleached garnet domains and localized deformation zones where dynamically recrystallized new garnet grains occur (Fig. 3e,f). The highly deformed host adjacent to the recrystallization zones is nearly inclusion-free. In the less deformed garnet domains the numerous inclusions reach only <1 μm grain size. It is supposed that within the deformation zones apatite, xenotime and rutile grew at expense of these primary magmatic very fine-grained inclusions of Na–Mg-bearing Ca-phosphate, xenotime and ilmenorutile–struverite. Obviously both P and Ti were able to migrate through the garnet crystal lattice of garnet domains adjacent to the deformation zones. We suggest that within the deformation zones diffusion was enhanced, thus enabling grain growth of the accessory phases. As xenotime and phosphates were already present during the magmatic stage, mineral reactions involving P- or Y-content in garnet (Pyle and Spear, 1999; Yang and Rivers, 2002) are not necessarily required for xenotime and apatite growth in the deformation zones. Besides, the limited Y-solubility in garnet at temperature conditions above 650 °C (Pyle and Spear, 1999), indicates that the primary Y-content of magmatic garnet was subordinate.

The restricted appearance and the preferred orientation of kyanite rods in deformation zones I (Fig. 3b) indicate that the localized plastic deformation triggered the (re)crystallization process. Since no lattice deformation of kyanite is evident where these crystals extend from the deformation zone into the relatively undeformed host, post-kinematic continuous crystallization (relative to plastic garnet deformation) is supposed to have occurred after syn-kinematic nucleation. Due to the peraluminous melt composition very fine-grained syn-magmatic Al_2SiO_5 inclusions similar to xenotime and phosphates may have been present in the garnet core even though not identified during EMP investigation. Besides, the occurrence of magmatic andalusite give evidence of excess Al as is provided by corundum inclusions along trails tracing the microfractures in garnet. However, we are not able to explain the absence of kyanite in deformation zones II–IV. The occurrence and stability of kyanite in deformation zones in contrast with the magmatic equilibrium relationship of garnet and andalusite represents important information concerning the metamorphic conditions of deformation. Dynamically recrystallized feldspar and quartz together with kyanite aggregates in the matrix represent the mylonitic foliation deflected around garnet, which has developed during the Cretaceous eclogite facies metamorphic event.

6.3. Metamorphic conditions of deformation

Deformation zones occur within the garnet core, but also cross-cut the weakly colored garnet rim, thus indicating that the major deformation postdated the entire garnet crystallization. Whereas the magmatic coarse-grained assemblage, including the cm-sized garnets, had formed at low pressure conditions of >650 °C/<0.4 GPa in equilibrium with andalusite (Clarke et al., 2005; Habler et al., 2007), the appearance of kyanite both in the matrix and within garnet indicates that the deformation took place at elevated P conditions. Metapelites in the wider study area of the southern Koralpe experienced their predominant deformational imprint during Cretaceous eclogite facies metamorphism. PT data from the wider study area concerning the Cretaceous pressure peak scatter significantly, given at 600–650 °C/1.8–2.0 GPa derived from eclogites and metapelites (Miller and Thöni, 1997), and at c. 640 °C or c. 710 °C based on different Zr in rutile thermometers, as well as 640–720 °C at a nominal pressure of 2.4 GPa using Grt-CPx thermometry (Miller et al., 2007). Major phase thermobarometry on metapelitic rocks yielded maximum Cretaceous metamorphic conditions at 700 ± 63 °C/1.5 ± 0.15 GPa (Tenczer and Stüwe, 2003).

Previous studies revealed fluid undersaturated conditions during the Cretaceous HP event in the Saualpe–Koralpe basement, causing only limited reaction progress (Tenczer et al., 2006). Fluid undersaturation is in line with the observation of dynamically recrystallized K-feldspar in the metapegmatites, although T conditions in the metapelitic pegmatite host rock generally did not exceed the muscovite stability during the Cretaceous HP event.

7. Summary and conclusions

Intracrystalline deformation zones in Permian magmatic garnets from a metapegmatite were analyzed in order to understand the deformation, recovery and recrystallization mechanisms and accompanied diffusion processes. The analyses of the deformation microstructures suggest the following.

1. Different deformation zones record the evolution of the microfabric of intracrystalline recrystallization of garnet.
2. Crystal plastic strain localization occurred (a) in response to the general flow stress around the garnet porphyroclast resulting in recrystallization zones parallel to each other and parallel to the foliation of the matrix, (b) along pre-existing or broadly synchronously developed fractures and (c) along heterogeneities across the growth zone between garnet core and quartz-rich outer margin.
3. Intragranular deformation zones are developed by localization of crystal plastic deformation, with associated recovery and subgrain rotation.
4. New grains of intragranular deformation zones within host garnet crystallographically oriented in an easy slip position have the same size as nearby subgrains and are developed by subgrain rotation recrystallization.
5. Recrystallized grains, once formed, partly underwent diffusion-accommodated grain boundary sliding, as evident by a randomization of neighbor grain misorientation axes and weakening of the CPO with ongoing deformation. However, grain boundary sliding did not operate to the exclusion of other mechanisms, like grain boundary migration and dislocation creep.
6. Deformation zones have also formed extensively along fractures or heterogeneities, e.g. across the growth zone between garnet core and quartz-rich outer margin. These deformation zones are suggested to represent sites of stress concentration. Higher internal strain energy, compared to deformation zones I, might have led to the weak CPO of new recrystallized grains due to a larger initial "rotation jump". Subsequent faster grain growth produced a coarser grain size compared to deformation zones I.
7. Diffusion processes in intragranular deformation zones were triggered by the process of dynamic recrystallization as indicated by slight but significant Ca variation across the deformation zones and the crystallization of apatite, xenotime and rutile within these zones.
8. There was no material exchange between the garnet interior and the matrix. Compositional variations in the intragranular deformation zones are a product of mineral reactions between garnet and very fine-grained magmatic inclusions

(Na–Mg-bearing Ca-phosphates, ilmenorutile–struverite, and xenotime).

9. The development of kyanite needles in the intracrystalline deformation zones, triggered by the localized crystal plasticity, indicates that the deformation occurred during major deformation of the metapelitic pegmatite host rock, which was related with Cretaceous eclogite facies metamorphism at H_2O undersaturated conditions.

Acknowledgments

We thank Bernhard Schulz and Bernhard Grasemann for stimulating discussions. Angela Halfpenny is acknowledged for SYTON polishing and coating of the thin section. T. Ntaflos is thanked for providing support with electron microprobe analyses. The manuscript was much improved by the reviews of Claudia Trepmann and Ghislain Trullenque. The study was funded by the Austrian research fund FWF in the projects P15644-N06 (main part) and T319-N10 (finalization). F.H. was supported by the EU Marie Curie Research Training Network 'c2c' (contract MRTN-CT-2006-035957).

References

Adams, B.L., Wright, S.I., Kunze, K., 1993. Orientation imaging: The emergence of a new microscopy. Metallurgical Transactions 24A, 819–831.

Ashby, M.F., Verrall, R.A., 1973. Diffusion accommodated flow and superplasticity. Acta Metallurgica 21, 149–163.

Bestmann, M., Prior, D.J., 2003. Intragranular dynamic recrystallization in naturally deformed calcite marble: diffusion accommodated grain boundary sliding as a result of subgrain rotation recrystallization. Journal of Structural Geology 25, 1597–1613.

Bestmann, M., Prior, D.J., Grasemann, B., 2006. Characterisation of deformation and flow mechanics around porphyroclasts in a calcite marble ultramylonite by means of EBSD analysis. Tectonophysics 413, 185–200.

Casey, M., Kunze, K., Olgaard, D.L., 1998. Texture of Solnhofen limestone deformed to high strains in torsion. Journal of Structural Geology 20, 255–267.

Clarke, D.B., Dorais, M., Barbarin, B., Barker, D., Cesare, B., Clarke, G., EL Baghdadi, M., Erdmann, S., Forster, H.-J., Gaeta, M., Gottesmann, B., Jamieson, R.A., Kontak, D.J., Koller, F., Leal Gomes, C., London, D., Morgan, G.B., Neves, L., Pattison, D.R.M., Pereira, A.J.S.C., Pichavant, M., Rapela, C.W., Renno, A.D., Richards, S., Roberts, M., Rottura, A., Saavedra, J., Sial, A.N., Toselli, A.J., Ugidos, J.M., Uher, P., Villaseca, C., Visona, D., Whitney, D.L., Williamson, B., Woodward, H. H., 2005. Occurrence and origin of andalusite in peraluminous felsic igneous rocks. Journal of Petrology 46, 441–472.

Den Brok, B., Kruhl, J.H., 1996. Ductility of garnet as an indicator of extremely high temperature deformation: Discussion. Journal of Structural Geology 18, 1369–1373.

Dobbs, H.T., Peruzzo, L., Seno, F., Spiess, R., Prior, D.J., 2003. Unraveling the Schneeberg garnet puzzle: a numerical model of multiple nucleation and coalescence. Contributions to Mineralogy and Petrology 146, 1–9.

Drury, M.R., Humphreys, F.J., White, S.H., 1985. Large strain deformation studies using polycrystalline magnesium as a rock analogue, Part II. Dynamic recrystallization mechanisms at high temperatures. Physical Earth Planetary Science 40, 208–222.

Faryad, S.W., Hoinkes, G., 2003. P-T gradient of Eo-Alpine metamorphism within the Austroalpine basement units east of the Tauern Window (Austria). Mineralogy and Petrology 77, 129–159.

Frey, M., Desmons, J., Neubauer, F., 1999. The new metamorphic map of the Alps. Schweizerische Mineralogische und Petrographische Mitteilungen 79 (1).

Fynn, G.W., Powell, W.J.A., 1979. The Cutting and Polishing of Electrooptic Materials. Adams Hilger, London.

Gifkins, R.C., 1973. Superplasticity, creep and grain-boundary sliding. Scripta Metallurgica 7, 27–33.

Gifkins, R.C., 1976. Grain-boundary sliding and its accommodation during creep and superplasticity. Metallurgical Transactions A—Physical Metallurgy and Materials Science 7, 1225–1232.

Gifkins, R.C., 1991. Ductility and strain-rate control mechanisms in superplasticity. Scripta Metallurgica et Materialia 25, 1397–1400.

Gifkins, R.C., 1994. Grain-boundary participation in high temperature deformation: an historical review. Materials Characterization 32, 59–77.

Gregurek, D., Abart, R., Hoinkes, G., 1997. Contrasting Eoalpine P-T evolutions in the southern Koralpe, Eastern Alps. Mineralogy and Petrology 60, 61–80.

Habler, G., Thöni, M., 2001. Preservation of Permo-Triassic low-pressure assemblages in the cretaceous high-pressure metamorphic Saualpe crystalline basement (Eastern Alps, Austria). Journal of metamorphic Geology 19, 679–697.

Habler, G., Thöni, M., Miller, C., 2007. Major and trace element chemistry and Sm-Nd age correlation of magmatic pegmatite garnet overprinted by eclogite-facies metamorphism. Chemical Geology 241, 4–22.

Humphreys, F.J., Bate, P.S., Hurley, P.J., 2001. Orientation averaging of EBSD data. Journal of Microscopy 201, 50–58.

Jessell, M.W., 1987. Grain-boundary migration microstructures in naturally deformed quartzite. Journal of Structural Geology 9, 1007–1014.

Ji, S.C., Martignole, J., 1994. Ductility of garnet as an indicator of extremely high-temperature deformation. Journal of Structural Geology 16, 985–996.

Jiang, Z., Prior, D., Wheeler, J., 2000. Albite crystallographic preferred orientation and grain misorientation distribution in a low-grade mylonite: implication for granular flow. Journal of Structural Geology 22, 1663–1674.

Karato, S., Wang, Z.C., Liu, B., Fujino, K., 1995. Plastic deformation of garnets: systematics and implications for the rheology of the mantle transition zone. Earth and Planetary Science Letters 130, 13–30.

Kleinschrodt, R., Duyster, J.P., 2002. HT-deformation of garnet: an EBSD study on granulites from Sri Lanka, India and the Ivrea Zone. Journal of Structural Geology 24, 1829–1844.

Klein-schrodt, R., McGrew, A., 2000. Garnet plasticity in the lower continental crust: implications for deformation mechanisms based on microstructures and SEM-electron channeling pattern analysis. Journal of Structural Geology 22, 795–809.

Kruse, R., Stuenitz, H., Kunze, K., 2001. Dynamic recrystallization processes in plagioclase porphyroclasts. Journal of Structural Geology 23, 1781–1802.

Leiss, B., Barber, D.J., 1999. Mechanisms of dynamic recrystallization in naturally deformed dolomite inferred from EBSP-analyses. Tectonophysics 303, 51–69.

Li, L., Long, H., Raterron, P., Weidner, D., 2006. Plastic flow of pyrope at mantle pressure and temperature. American Mineralogist 91, 517–525.

Lloyd, G.E., 1987. Atomic number and crystallographic contrast images with the SEM: a review of backscatter techniques. Mineralogical Magazine 51, 3–19.

Lloyd, G.E., Freeman, B., 1994. Dynamic recrystallization of quartz and quartzites. Journal of Structural Geology 16, 867–881.

Lloyd, G.E., Farmer, A.B., Mainprice, D., 1997. Misorientation analysis and the formation and orientation of subgrain and grain boundaries. Tectonophysics 279, 55–78.

Loomis, T.P., Ganguly, J., Elphick, S.C., 1985. Experimental determination of cation diffusivities in aluminosilicate garnets. Contribution of Mineralogy and Petrology 90, 45–51.

Miller, C., Thöni, M., 1997. Eo-Alpine eclogitisation of Permian MORB-type gabbros in the Koralpe (Eastern Alps, Austria): new geochronological, geochemical and petrological data. Chemical Geology 137, 283–310.

Miller, C., Zanetti, A., Thöni, M., Konzett, J., 2007. Eclogitisation of gabbroic rocks: redistribution of trace elements and Zr in rutile thermometry in an Eo-Alpine subduction zone (Eastern Alps). Chemical Geology 239, 96–123.

Pouchou, J.-L., Pichoir, F., 1991. Quantitative analysis of homogeneous or stratified microvolumes applying the model "PAP". In: Heinrich, K.F.J., Newbury, D.E. (Eds.), Electron Probe Quantitation. Plenum, New York, pp. 31–75.

Pyle, J.M., Spear, F.S., 1999. Yttrium zoning in garnet: Coupling of major and accessory phases during metamorphic reactions. Geological Materials Research 1, 49.

Prior, D.J., 1999. Problems in determining the misorientation axes, for small angular misorientations, using electron backscatter diffraction in the SEM. Journal of Microscopy 195, 217–225.

Prior, D.J., Trimby, P.W., Weber, U.D., Dingley, D.J., 1996. Orientation contrast imaging of microstructures in rocks using forescatter detectors in the scanning electron microscope. Mineralogical Magazine 60, 859–869.

Prior, D.J., Wheeler, J., Brenker, F.E., Harte, B., Matthews, M., 2000. Crystal plasticity of natural garnet: new microstructural evidence. Geology 28, 1003–1006.

Prior, D.J., Wheeler, J., Peruzzo, L., Spiess, R., Storey, C., 2002. Some garnet micro structures: an illustration of the potential of orientation maps and misorientation analysis in microstructural studies. Journal of Structural Geology 24, 999–1011.

Ree, J.H., 2000. Grain boundary sliding in experimental deformation of octachloropropane. In: Jessel, M.W., Urai, J.L. (Eds.), Stress, Strain and Structure, A Volume in Honor of W.D. Means. Jounal of Virtual Explorer 2.

Sammis, C.G., 2001. Materials science issues in the Earth and Planetary sciences. Progress in Materials Science 46, 231–247.

Schmid, S.M., Fügenschuh, B., Kissling, E., Schuster, R., 2004. Tectonic map and overall architecture of the Alpine orogen. Eclogae Geologicae Helvetiae 97, 93–117.

Schmidt, N.H., Bildesorensen, J.B., Jensen, D.J., 1991. Band positions used for online crystallographic orientation determination from electron back scattering patterns. Scanning Microscopy 5, 637–643.

Schwandt, C.S., Papike, J.J., Shearer, C.K., 1996. Trace element zoning in pelitic garnet of the Black Hills, South Dakota. American Mineralogist 81, 1195–1207.

Schuster, R., Scharbert, S., Abart, R., Frank, W., 2001. Permo-Triassic extension and related HT/LP metamorphism in the Austroalpine-Southalpine realm. Mitteilungen der Gesellschaft der Geologie- und Bergbaustudenten Österreichs 45, 111–141.

Spiess, R., Peruzzo, L., Prior, D.J., Wheeler, J., 2001. Development of garnet porphyroblasts by multiple nucleation, coalescence and boundary misorientation-driven rotations. Journal of Metamorphic Geology 19, 269–290.

Storey, C.D., Prior, D.J., 2005. Plastic deformation and recrystallization of garnet: a mechanism to facilitate diffusion creep. Journal of Petrology 46, 2593–2613.

Tenczer, V., Stüwe, K., 2003. The metamorphic field gradient in the eclogite type locality Koralpe region, Eastern Alps. Journal of Metamorphic Geology 21, 377–393.

Tenczer, V., Powell, R., Stüwe, K., 2006. Evolution of H2O content in a polymetamorphic terrain: The Plattengneiss Shear Zone (Koralpe, Austria). Journal Metamorphic Geology 24, 281–295.

Terry, M.P., Heidelbach, F., 2004. Superplasticity in garnet from eclogite facies shear zones in the Haram Gebbro, Haramsøya. Norway. Geology 32, 281–284.

Thöni, M., Miller, C., 2000. Permo-Triassic pegmatites in the eo-Alpine eclogite-facies Koralpe complex, Austria: age and magma source constraints from mineral chemical, Rb-Sr and Sm-Nd isotope data. Schweizerische Mineralogische und Petrogrologische Mitteilungen 80, 169–186.

Thöni, M., Miller, Ch., Zanetti, A., Habler, G., Goessler, W. Sm-Nd isotope systematics of high-REE accessory minerals and major phases: ID-TIMS, LA-ICP-MS and EPMA data constrain multiple Permian-Triassic pegmatite emplacement in the Koralpe, Eastern Alps. Chemical Geology, in press.

Trepmann, C.A., Stöckhert, B., 2002. Cataclastic deformation of garnet: a record of synseismic loading and postseismic creep. Journal of Structural Geology 24, 1845–1856.

Trepmann, C.A., Stöckhert, B., Dorner, D., Hamidzadeh Moghadam, R., Küster, M., Röller, K., 2007. Simulating coseismic deformation of quartz in the middle crust and fabric evolution during postseismic stress relaxation—An experimental study. Tectonophysics 442, 83–104.

Urai, J.L., Jessell, M., 2001. Recrystallization and grain growth in minerals: recent developments. In: Gottstein, G., Molodov, D. (Eds.), Proceedings of the First Joint International Conference on Recrystallization and Grain Growth. Springer, Berlin, pp. 87–95.

Urai, J.L., Means, W.D., Lister, G.S., 1986. Dynamic recrystallization of minerals. In: Hobbs, B.E., Heard, H.C. (Eds.), Mineral and Rock Deformation (Laboratory Studies). Geophysical Monograph, 36, pp. 161–200. American Geophysical Union.

Voegele, V., Ando, J.I., Cordier, P., Liebermann, R.C., 1998a. Plastic deformation of silicate garnets I: high-pressure experiments. Physics of the Earth and Planetary Interiors 108, 305–318.

Voegele, V., Cordier, P., Sautter, V., Sharp, T.G., Lardeaux, J.M., Marques, F.O., 1998b. Plastic deformation of silicate garnets II: deformation microstructures in natural samples. Physics of the Earth and Planetary Interiors 108, 319–338.

Wheeler, J., Prior, D.J., Jiang, Z., Spiess, R., Trimby, P.J., 2001. The petrological significance of misorientations between grains. Contributions to Mineralogy and Petrology 141, 109–124.

Whitworth, M.P., Feely, M., 1994. The compositional range of magmatic Mn-garnets in the Galway Granite, Connemara, Ireland. Mineralogical Magazine 58, 163–168.

Yang, P., Rivers, T., 2002. The origin of Mn and Y annuli in garnet and the thermal dependence of P in garnet and Y in apatite in calc-pelite and pelite, Gagnon terrane, western Labrador. Geological Materials Research 4 (1), 1–25.